processes

MDPI

Article

Formulation of Nucleic Acids by Encapsulation in Lipid Nanoparticles for Continuous Production of mRNA

Alina Hengelbrock, Axel Schmidt and Jochen Strube *

Institute for Separation and Process Technology, Clausthal University of Technology, Leibnizstr. 15, 38678 Clausthal-Zellerfeld, Germany; hengelbrock@itv.tu-clausthal.de (A.H.); schmidt@itv.tu-clausthal.de (A.S.)
* Correspondence: strube@itv.tu-clausthal.de

Abstract: The development and optimization of lipid nanoparticle (LNP) formulations through hydrodynamic mixing is critical for ensuring the efficient and cost-effective supply of vaccines. Continuous LNP formation through microfluidic mixing can overcome manufacturing bottlenecks and enable the production of nucleic acid vaccines and therapeutics. Predictive process models developed within a QbD Biopharma 4.0 approach can ensure the quality and consistency of the manufacturing process. This study highlights the importance of continuous LNP formation through microfluidic mixing in ensuring high-quality, in-specification production. Both empty and nucleic acid-loaded LNPs are characterized, followed by a TFF/buffer exchange to obtain process parameters for the envisioned continuous SPTFF. It is shown that LNP generation by pipetting leads to a less preferable product when compared to continuous mixing due to the heterogeneity and large particle size of the resulting LNPs (86–104 nm). Particle size by continuous formation (71 nm) and the achieved encapsulation efficiency (EE) of 88% is close to the targeted parameters for Pfizer's mRNA vaccine (66–93 nm, 88%EE). With the continuous encapsulation of nucleic acids in LNPs and the continuous production of mRNA in in vitro transcription, the basis for the holistic continuous production of mRNA is now established. We already showed that a fully autonomous process requires the incorporation of digital twins and a control strategy, with predictive process models and state-of-the-art PAT enabling real-time-release testing. This autonomous control can considerably improve productivity by about 15–20% and personnel as well as chemical reduction of about 30%. The results of this work complement this, laying the basis for fully continuous, bottleneck-free production of mRNA and other cell- and gene-therapeutic drug/vaccine candidates in a GMP- and QbD-compliant Biopharma 4.0 facilities on a flexible scale.

Keywords: mRNA vaccine manufacturing; in vitro transcription; lipid nanoparticles; continuous biomanufacturing; digital twins; machine learning; autonomous operation

Citation: Hengelbrock, A.; Schmidt, A.; Strube, J. Formulation of Nucleic Acids by Encapsulation in Lipid Nanoparticles for Continuous Production of mRNA. *Processes* **2023**, *11*, 1718. https://doi.org/10.3390/pr11061718

Academic Editor: Sandra Balbino

Received: 27 April 2023
Revised: 15 May 2023
Accepted: 31 May 2023
Published: 4 June 2023

1. Introduction

The production of mRNA on a commercial scale has only recently been undertaken, with a focus on rapidly delivering the COVID-19 vaccines to the market and patients [1,2]. Due to this urgency, there has been little emphasis on process optimization, leaving room for significant improvements in various aspects of the production process. These aspects include plasmid production, in vitro transcription [3], purification [4], encapsulation [5], and storage and transport [6].

The reason why current commercial mRNA production batches are limited to a few hundred liters is due to constraints associated with the lipid-based encapsulation process utilized to generate lipid nanoparticles (LNPs). Because mRNA is highly sensitive, the duration of the encapsulation process must be minimized, thereby limiting the batch size [6].

Microfluidic mixing method has been identified as the most successful manufacturing technology for preparing lipid nanoparticles at a GMP scale [7]. However, the chaotic mixer

device is most widely used to prepare mRNA-LNPs [8]. Additionally, the manufacturing process for LNPs is complex and involves several different lipids at specific ratios, including some highly specialized ones, as well as organic solvents [6]. By changing the volume ratio or flow rate ratio between the two phases, the size of LNPs can be controlled [9].

This is especially important since the size of lipid nanoparticles used in drug delivery is a crucial factor affecting their biodistribution and uptake. Smaller particles between 20 and 150 nm are more effective at escaping kidney filtration and show initial aggregation effects in the liver and spleen, while larger particles above 150 nm are more likely to be trapped in these organs [10]. For subcutaneous injections, smaller particles are preferred as they facilitate uptake by lymphatic vessels and capillaries. Specifically, liposomes of 40 nm have a higher lymphatic uptake rate compared to larger particles, with approximately 76% of them being absorbed by the lymph nodes [11].

To ensure a timely and cost-effective supply of vaccines, it is crucial to continue developing and optimizing lipid nanoparticle (LNP) formulations through hydrodynamic mixing. This can be achieved through studies that examine LNP formation, both empty and with nucleic acid load, followed by TFF/buffer exchange to obtain process parameters for envisioned continuous SPTFF. This approach can help overcome manufacturing bottlenecks and enable the production of nucleic acid vaccines and therapeutics through continuous manufacturing that is controlled and optimized in real-time by PAT and Digital-Twins. The development of validated, predictive process models within a QbD Biopharma 4.0 approach can help ensure the quality and consistency of the manufacturing process. By investing in these advancements, we can secure a resilient and sustainable supply of vaccines and therapeutics for the future.

State-of-the-Art in Lipid Nanoparticle Manufacturing

The produced mRNA needs to be protected from early degradation to transport the mRNA into the cytosol of antigen-presenting cells and maintain its high efficacy [12–14]. This can be achieved using lipid nanoparticles. Lipid nanoparticles for the encapsulation of nucleic acids usually consist of four main components: an ionizable lipid, a sterol, a polyethylene glycol lipid (PEG lipid), and a neutral phospholipid. Ionizable lipid contains ionizable amine groups that are positively charged at low pH and can interact with the anionic nucleic acids to form particles. In addition to initiating particle formation, cationic ionizable lipid serves to facilitate membrane fusion during internalization [12,15–17]. The PEG lipid is thought to prevent aggregation during storage as the PEG chain is hydrophilic and thus coats the particle, acting as a steric barrier [18]. In addition, the PEG lipid serves to control the thermodynamically stable particle size. Thus, by increasing the amount of the PEG lipid in the lipid mixture, the particle size can be decreased [12,18,19]. The neutral phospholipid forms a bilayer just below the peripheral PEG layer in the LNPs and the sterol is present, distributed in the LNPs [18,19]. For the formulation, the nucleic acids are placed in aqueous buffer with a low pH and the lipids appear in an organic phase such as ethanol without counterions so that the ionizable lipid is uncharged [18]. When both solutions are mixed, nanoparticles form spontaneously due to hydrophobic and electrostatic interactions between the positively charged amine groups of the ionizable lipid and the negative charges of the phosphate backbone of the nucleic acid [18,20].

Figure 1 shows how LNPs could be formed and look like. The exact structure of the LNP core and its dependence on the lipid composition and the localization of the nucleic acids has not yet been conclusively clarified [12].

Various methods are available for the preparation of lipid nanoparticles. Former methods include thin-layer hydration and ethanol injection [16,18,21]. The simplest method for the preparation of LNPs on a laboratory scale is considered to be preparation via pipetting [21]. These three methods have the disadvantage of usually producing nanoparticles with heterogeneous, larger particles and low encapsulation efficiencies, and they are also difficult to scale up [16,18,21,22]. In developing the optimal formulation and formulation parameters, very small volumes in the µL range are generated by mixing in microfluidic

devices. However, larger batches are required for production scale manufacturing, so the mixing of the two solutions is generally performed using T-mixers. In this process, both methods can generate LNPs of similar size of <100 nm and morphology by rapid mixing [18,23]. Rapid mixing is achieved in the T-mixer by converting the laminar input flows into a turbulent flow at the mixing point with a Reynolds number of approximately 11,000 [24,25]. The size of the particles is particularly influenced by the total flow rate (TFR) and the flow ratio (FRR), in addition to the lipid composition [26]. For the encapsulation of the mRNA vaccine, usually one part lipid solution is mixed with three parts of the aqueous buffer containing the mRNA to be encapsulated [18].

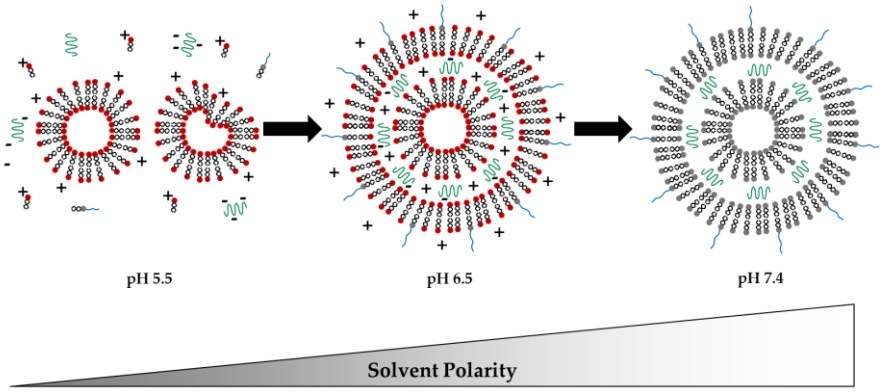

Figure 1. Schematic representation of what the spontaneous formation of lipid nanoparticles might look like, since the exact structure of LNPs has not yet been conclusively determined. LNPs consisting of an ionizable cationic lipid (lipids with red head at pH 5.5 and 6.5; and uncharged black head at pH 7.4), a PEG lipid (lipids with blue PEG chain at lipid head), a styrene and a neutral phospholipid (both not shown for simplification), and the drug substance (green helices), which is dependent on pH. The charge distribution is indicated with minus signs for negative charges and plus signs for positive charges.

In order to limit the particle size to <100 nm in the other production methods, methods such as extrusion or sonication are needed [18,26,27]. This is necessary because optimal uptake of the uncharged nanoparticles by the lymph nodes where the immune response is triggered occurs at a particle size of 10–100 nm [28].

After mixing the two phases, the ethanol must be removed and the pH raised so that the ionizable lipid is again uncharged. This can be achieved via dilution with aqueous buffer, dialysis or tangential flow filtration [18,23]. When the ionizable lipid is neutral again, it is less soluble. This leads to the formation of larger lipid domains, which accelerates the fusion process of the LNPs. As a result, the LNPs increase in size, so that up to 36 vesicles fuse to form a final LNP [18].

LNP formulation for (p)DNA delivery has been reported in the literature, e.g., for LNP systems as transfection reagents for plasmid DNA (pDNA) [29], for enahnced oral delivery of DNA [30], for increased efficiency of DNA-vectored vaccines/immunoprophylaxis in animals [31], for spherical nucleic acids for intracellular DNA and RNA delivery [32], for transfection of cell model lines [33], as nanocarrier to deliver a cancer vaccine against the benchmark target tyrosine-kinase receptor HER2 in C57BL/6 mice [34], as well as in evaluating studies regarding the role of the influential Microfluidic Formulation of DNA-Loaded Multicomponent Lipid Nanoparticles for Gene Delivery factors [26].

2. Materials and Methods

2.1. pDNA Production

The pDNA encoding the mRNA BNT162b2 was produced via fermentation of *E.coli* in a 2.5 L bioreactor (Sartorius, Göttingen, Germany). After cell harvest via centrifugation, alkaline lysis of the cells was followed by UF/DF to concentrate the pDNA and exchange the

buffer. Subsequently, the pDNA was further purified using an anion exchanger (Fractogel® EMD DEAE, Merck Millipore, Burlington, MA, USA) and finally transferred in a 50 mM sodium citrate buffer at pH4 using UF/DF. For linearized pDNA, after the chromatography step, the pDNA was buffered into the reaction buffer for subsequent linearization with the EcoRI restriction enzyme (Thermo ScientificTM, Waltham, MA, USA) before the linearized pDNA was transferred into the acidic aqueous buffer.

2.2. Formulation of LNPs

The formation of the LNPs is first carried out in a batchwise manner via pipetting. Empty LNPs were prepared as positive control. Encapsulation of linearized pDNA was performed as it is present in the reaction mix for in vitro transcription. For this, the experimental plan shown in Table 1 was carried out, with all experiments performed on a 1.5 mL scale and experiments 0 and 1 additionally on a 0.5 mL scale. An ionizable lipid (ALC-0315; Cayman Chemical, Ann Arvor, MI, USA), a sterol (cholesterol; Cayman Chemical, Ann Arvor, MI, USA), a PEG lipid (ALC-0159; Cayman Chemical, Ann Arvor, MI, USA), and a phospholipid (1,2-distearoyl-sn-glycero-3-phosphocholine, DSPC; Avanti Polar Lipids, Alabaster, AL, USA) were used for the formulation. Since the encapsulated pDNA encodes the BNT162b2 mRNA, the molar ratios of the lipids in the lipid mix were also based on the Pfizer/BioNTech mRNA vaccine formulation [12,35].

Table 1. Experimental plan for the LNP formulation.

Exp. No.	mRNA/pDNA	mRNA/pDNA (mg/mL)	Ion. Lipid (mg/mL)	PEG-Lipid (mg/mL)	DSPC (mg/mL)	Cholesterol (mg/mL)
0	(pos. control)	0	11.8	1.4	2.5	5.5
1	pDNA	0.27	11.8	1.4	2.5	5.5
2	lin. pDNA	0.27	11.8	1.4	2.5	5.5

Subsequently, the scale-up for the continuous LNP formulation took place. For this, a total of 12 mL was mixed rapidly with a flow rate ratio of 3:1 (aqueous:organic) in a T-mixer. The continuous LNP formulation took place in the facility shown in Figure 2.

Figure 2. Set-up of the mixing section for the continuous LNP formulation.

2.3. Analytics of LNP

For the encapsulated nucleic acids in LNPs, there are several critical quality attributes (CQAs; see Table 2) that must be within a defined range for the product to be released. These CQAs are derived from the quality target product profile (QTPP). It includes the intended

clinical use, route of administration, dose, type of lipid nanosystem, and final product quality, safety, and efficacy [36,37]. As this study is based on the Pfizer/BionTech studies, the clinical application is a vaccine with a dose of 30 µg administered intramuscularly and encapsulated in lipid nanoparticles [35].

The CQAs can be determined by different analytical methods. For LNP, most methods are based on the evaluation of the MALS/DLS signal in combination of a separation. For the separation of particles according to their size, flow field fractionation (FFF) and size exclusion chromatography (SEC) are the main methods listed in the literature [38–45]. In addition to MALS/DLS, UV and RI detectors are used for the detection of LNP. Encapsulation efficiency (EE) can be determined via chromatographic methods such as ion exchange chromatography (IEX), reversed phase chromatography (RP) or SEC [39,40,46]. In addition, a ribogreen assay or cryo-electron microscopy can be used (Cryo-EM) [39,40,47]. For LNP properties such as lipid identity, composition- and lipid-related impurities as well as LNP morphology, no acceptance criteria are currently documented [39].

Table 2. Critical Quality Attributes for LNP Formulation [39].

Quality Attribute	Acceptance Criteria
Encapsulation Efficiency	>80%
LNP Size	<100 nm
Polydispersity Index	<0.3
LNP Charge	±20 mV
Lipid Identity and Content, Lipid-related Impurities	N/A
LNP Morphology	N/A

2.3.1. Encapsulation Efficiency

The encapsulation efficiency is determined using the anion exchange chromatography TSKgel® DNA-NPR (7.5 cm × 4.6 mm, 2.5 µm particle size; Tosoh Bioscience, Tokyo, Japan). For this purpose, the LNP sample is measured without pretreatment and followed by lysis. Lysis of LNP is induced by the addition of Triton X-100 as described in the literature [26,33,48,49] and the pDNA peak is analyzed by area. The encapsulation efficiency can then be determined using the following formula [26,33]:

$$EE = \frac{A_{Lysed\ LNP} - A_{Not\ Lysed\ LNP}}{A_{Lysed\ LNP}} \cdot 100. \quad (1)$$

2.3.2. Size Characterization

The size and size distribution of the generated LNPs is determined by SEC-MALS/DLS. Size exclusion chromatography is performed using TSKgel G5000PWxl-CP (Tosoh Bioscience, Tokyo, Japan). The modified particles of the column are positively charged and thus can prevent interactions of LNPs with the resin [45]. 1xPBS at pH is used as the mobile phase and isocratically pumped through the system at a flow rate of 0.3 mL/min. After the LNP exit the column, the LNP sample passes through a UV detector and the MALS/DLS detector (DAWN®; Wyatt Technology Corporation, Santa Barbara, CA, USA). The latter, in combination with the Astra software (version 8.1.1; Wyatt Technologie Corporation, Santa Barbara, CA, USA), enables the determination of particle sizes (distribution). This determines the temporal variance σ_i from the elution profile and subsequently the molecular diffusion coefficient D_i from this using Equation (2) and knowledge of the capillary radius R_c of the capillary used and the elution time t_0 [50].

$$D_i = \frac{{R_C}^2 \cdot t_0}{24 \cdot {\sigma_i}^2}. \quad (2)$$

Using the Boltzmann constant k_B, the temperature T and the viscosity of the eluent η, the hydrodynamic diameter $D_{h,i}$ can be calculated with the Stokes–Einstein equation [50].

$$D_{h,i} = \frac{k_B \cdot T}{6 \cdot \pi \cdot \eta \cdot D_i}. \quad (3)$$

Knowing the standard deviation of the hydrodynamic diameter σ_{D_h} (Equation (4)) and the mean hydrodynamic diameter $\overline{D_h}$, the polydispersity index (PDI) can be determined using Equation (5) [50].

$${\sigma_{D_h}}^2 = \frac{\int_{D_{hmin}}^{D_{hmax}} \left(D_h - \overline{D_h}\right)^2 P(D_h) dD_h}{\int_{D_{hmin}}^{D_{hmax}} P(D_h) dD_h}. \quad (4)$$

$$PDI = \left(\frac{\sigma_{D_h}}{\overline{D_h}}\right)^2. \quad (5)$$

2.4. Ultra-/Diafiltration

The TFF set-up for the scalable mRNA machine published by Hengelbrock et al. [51] was also used in this work, with slight modifications. The exchange buffer (1X PBS, pH 7.4) was continuously added by a HPLC pump (Knauer K501, KNAUER Wissenschaftliche Geräte GmbH, Berlin, Germany) with a permeate matching flow rate to keep the total volume constant. A total of 9 diavolumes were used for buffer exchange, which corresponds to a buffer exchange of more than 99%. The examined hollow fiber module (Type C02-E100-05-S, Repligen Corporation, Boston, MA, USA) has an effective length of 200 mm and a fiber inner diameter of 0.5 mm. With 6 fibers, this results in an effective filter area of 20 cm^2. The fiber material is mPES (modified polyethersulfone) and the MWCO (molecular weight cut-off) is 100 kDa.

The mean pressure on the feed side can be calculated as the average of the feed pressure P_F and the retentate pressure P_{Ret}. The difference between the mean pressure on the feed side and the permeate side is known as the transmembrane pressure (TMP) (as shown in (Equation (6)). In order to maintain optimal conditions, the TMP is regulated throughout the process using a control valve (see Figure 3).

$$TMP = \frac{P_F + P_{Ret}}{2} - P_{Per}. \quad (6)$$

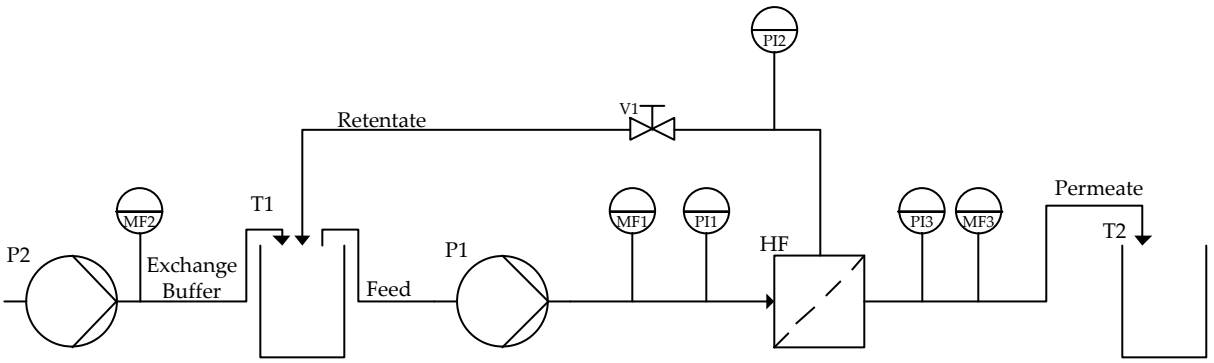

Figure 3. Ultra-/diafiltration process flowsheet. T1 (feed reservoir), P1 (feed pump), P2 (exchange buffer pump), MF1 (feed mass flow indicator), PI1 (feed pressure indicator), HF (hollow fiber module), PI2 (retentate pressure indicator), V1 (pressure control valve), PI3 (permeate pressure indicator), MF2 (exchange buffer mass flow indicator), MF3 (exchange buffer mass flow indicator), T2 (permeate tank).

Equation (7) calculates the permeate flux LMH, which is obtained by normalizing the permeate flow flow $\dot{V}_{Per}$ to the membrane area A_{Mem}:

$$LMH = \frac{\dot{V}_{Per}}{A_{Mem}}. \quad (7)$$

Equation (8) can be used to calculate the apparent sieving coefficient $S_{app,i}$, which indicates the relative concentrations of component i in the feed $c_{F,i}$ and permeate $c_{Per,i}$ [52]:

$$S_{app,i} = \frac{c_{Per,i}}{c_{F,i}}. \quad (8)$$

By using the apparent sieving coefficient $S_{app,i}$ it is possible to calculate the apparent retention of component i $R_{app,i}$ in the process via $S_{app,i}$ by Equation (9):

$$R_{app,i} = 1 - S_{app,i}. \quad (9)$$

The concentration increase in the retained components in the retentate is given by the volume concentration factor VCF as shown in Equation (10) [53].

$$VCF = \frac{V_{F,start}}{V_{Ret,end}}. \quad (10)$$

The focus of the study was to characterize the separation of ethanol, leftover lipids, and non-encapsulated nucleic acids as well as the neutralization towards the target pH value of 7.4. The mixed LNP solution after passing the T-mixer was initially combined with a 2 DV exchange buffer to stop the LNP formation reaction. This diluted solution was initially concentrated back to a VCF of 1, before starting the continuous buffer exchange. The initial volume $V_{F,start}$ thus equals the final volume of retentate $V_{Ret,end}$.

3. Results

3.1. LNP Formation in Batch

In order to demonstrate the feasibility of the LNP formulation, small-scale experiments were first performed in batch. The influence of the scale from 0.5 mL to 1.5 mL and the influence of the encapsulated nucleic acid were investigated. The chromatograms of SEC and AEX analysis and particle size analysis by MALS/DLS for empty and pDNA-loaded LNP in a 0.5 mL scale are shown in Figure 4**.** The low maximum UV signal of approximately 11 mAU for empty LNPs and approximately 2 mAU for LNP with pDNA, respectively, and the low DLS count rate of 2.8×10^6 (empty LNP) and 5.4×10^5 (pDNA LNP), respectively, suggest that few LNPs are generated in the 0.5 mL scale. With a hydrodynamic radius range of 44 nm to 69 nm (empty) and 45 nm to 66 nm (pDNA), respectively, heterogeneous particle size distributions are present. Moreover, the mean hydrodynamic radius of 52 ± 6 nm for the empty LNPs and the LNPs with pDNA, corresponding to a particle size of 104 nm, is larger than the maximum particle size of 100 nm allowed by QA. This results in a polidispersity index of 0.012 for both the empty LNP and the LNP with pDNA, which, on the in contrast, fulfills the QA requirements.

Although LNPs were generated in the 0.5 mL scale, they were only slightly concentrated, possibly due to the challenging handling of the small volumes, which at 0.5 mL is close to the dead volume of the hollow fiber module of 0.3 mL. Therefore, to investigate the influence of scale on particle size and encapsulation efficiency, the batch approach was tripled to a total of 1.5 mL.

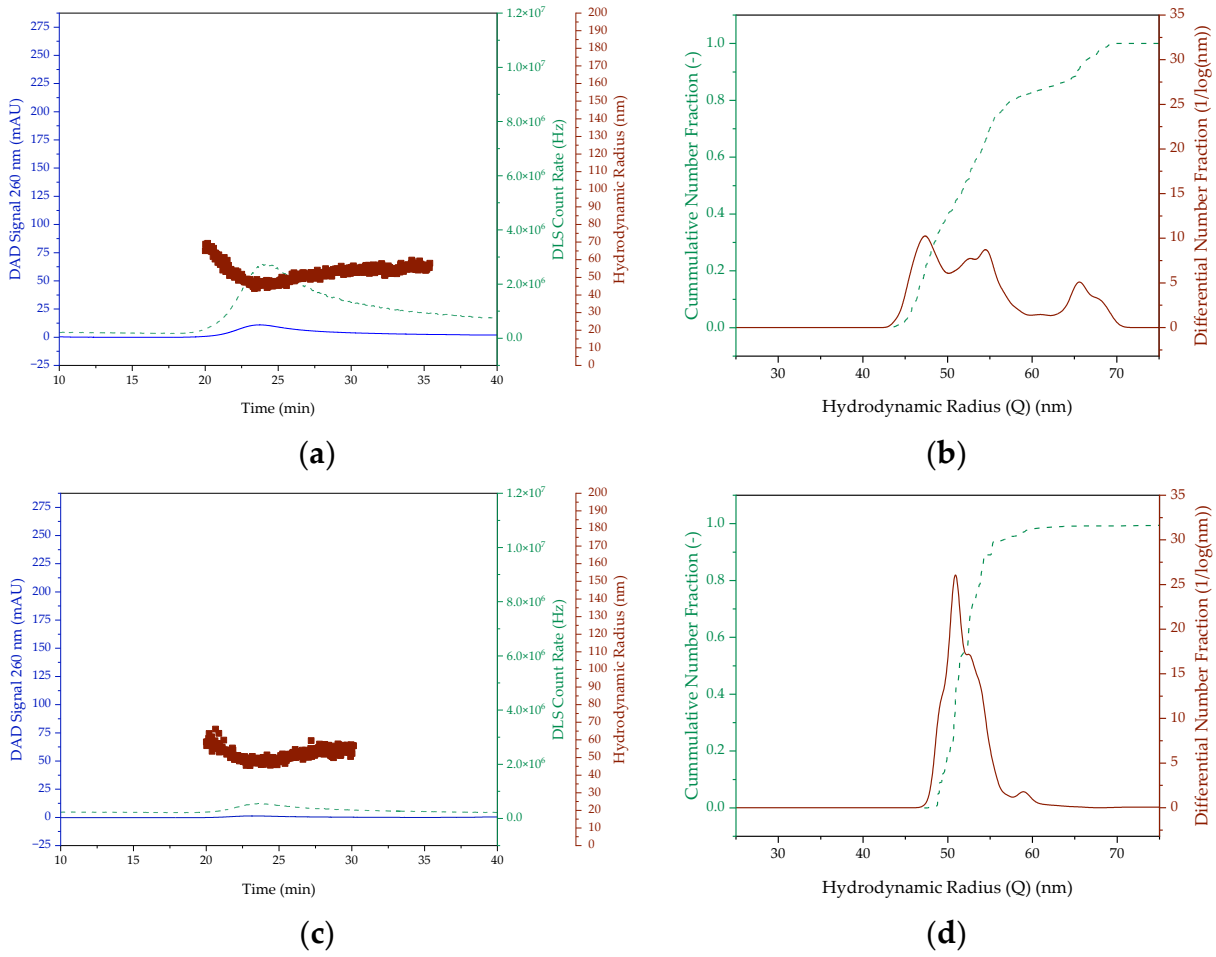

Figure 4. SEC chromatogram and DLS signal ((**a**,**b**) empty) as well as the cumulative and differential distribution of hydrodynamic radius ((**c**,**d**) pDNA) of LNP prepared batchwise in 0.5 mL scale. The DAD Signal is colored blue. In (**a**,**c**), the red colored dots represent the hydrodynamic radius and the green dashed lines represent the DLS Count Rate. In (**b**,**d**), however, the green dashed line is the cumulative number fraction and the red line is the differential number fraction.

Figure 5 shows the analytical results of the LNP formulations with and without pDNA in the 1.5 mL scale. In contrast to the 0.5 mL approach, the UV signal is stronger by a factor of 2.5 (empty LNP) and 129 (LNP containing pDNA). In addition, a higher DLS count rate by a factor of 2 (empty) and 19 (pDNA) is observed. Both indicate a significantly higher particle concentration than in the 0.5 mL scale. Thus, the mean hydrodynamic radii of 48 $\pm$ 6 nm for the empty nanoparticles and 43 $\pm$ 4 nm for the nanoparticles loaded with pDNA are slightly smaller than in the 0.5 mL scale. This indicates a higher mixing speed, which has a positive effect on particle size [24,25,54] during pipetting. The particle size ranges of 39 to 69 nm (empty) and 34 to 63 nm (pDNA) also deviate accordingly from those in the smaller scale. The maximum particle size has not changed, but the minimum particle size has become smaller, resulting in a broader distribution and a PDI of 0.02. Thus, more particles meet the quality criteria, but are still at the limit of the maximum permissible particle size. In contrast to the size, the achieved encapsulation efficiency of the pDNA of 90% is not critical, as it is significantly above the minimum permissible EE of 80%.

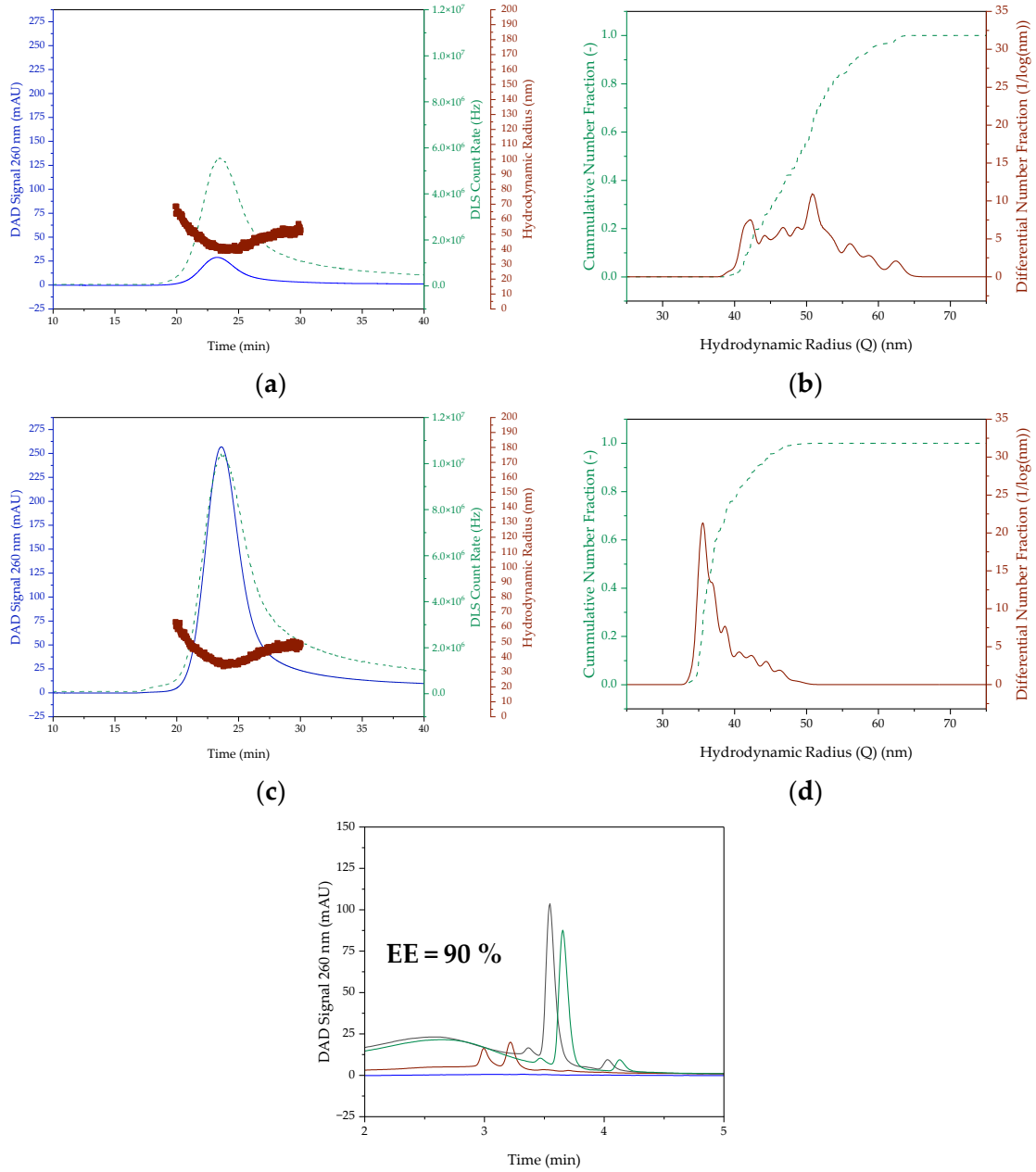

Figure 5. SEC chromatogram and DLS signal ((**a**,**b**) empty) as well as the cumulative and differential distribution of hydrodynamic radius ((**c**,**d**) pDNA) of LNP prepared batchwise in 1.5 mL scale. (**e**) Encapsulation efficiency of pDNA containing LNP. The DAD Signal is colored blue. In (**a**,**c**), the red colored dots represent the hydrodynamic radius and the green dashed lines represent the DLS Count Rate. In (**b**,**d**), however, the green dashed line is the cumulative number fraction and the red line is the differential number fraction. In (**e**), the black line represents the feed solution chromatogram, the blue line is the permeate and the green and red line represent the retentate, with the green line being the retentate treated with Triton.

In order to additionally investigate the influence of the encapsulated nucleic acid, linearized pDNA was encapsulated in addition to pDNA. Although this is not used as a therapeutic agent, it serves as a template as a starting point for mRNA formulation. Consequently, it plays a central role in in vitro transcription. In contrast to the encapsulation of pDNA in the 1.5 mL scale, the UV signal and DLS count rate are lower by a factor of four and two, respectively (cf. Figure 6). With a mean hydrodynamic radius of 60 ± 10 nm, the

particles are significantly larger than the other batch-prepared LNPs. The particle size varies from 36 nm to 75 nm, indicating a much broader distribution. This also indicates the PDI with a value of 0.027. In addition, the encapsulation efficiency of 32% is significantly lower than that achieved with pDNA encapsulation. Reasons for this could be the simultaneous presence of linearized, non-linearized and incompletely linearized pDNA as well as the presence of any impurities caused by the linearization enzyme.

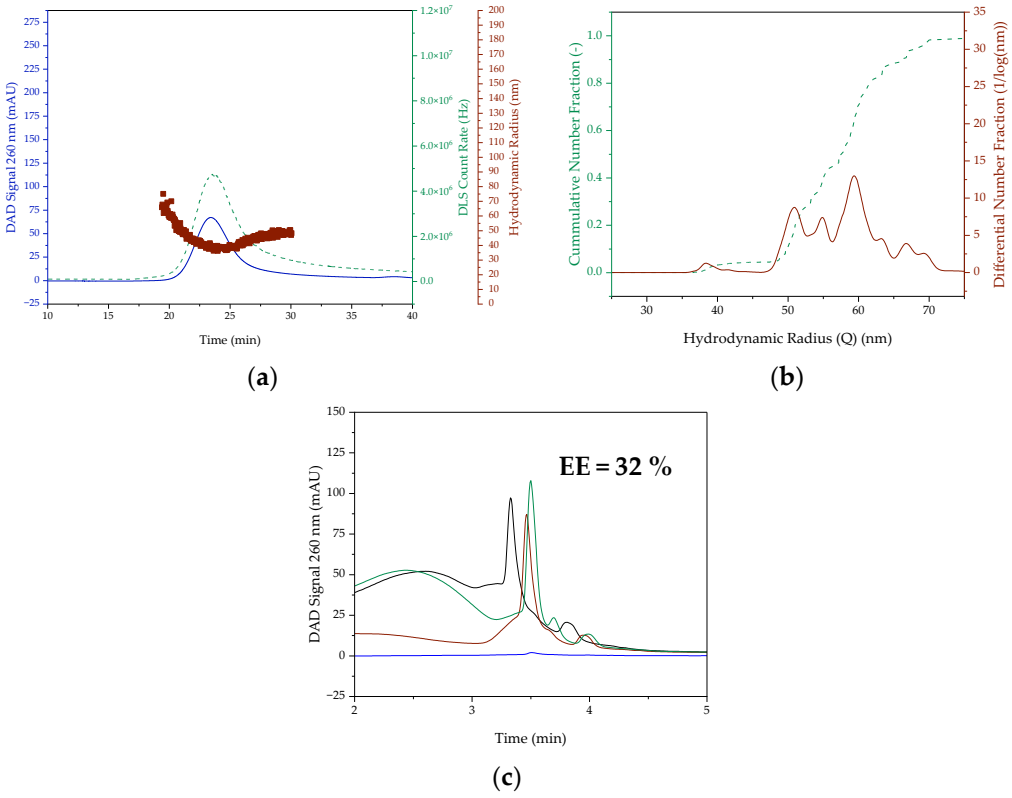

Figure 6. (**a**) SEC chromatogram and DLS signal as well as (**b**) the cumulative and distribution of hydrodynamic radius of LNP with linearized pDNA prepared batchwise in 1.5 mL scale. (**c**) Encapsulation efficiency of linearized pDNA containing LNP. The DAD Signal is colored blue. In (**a**), the red colored dots represent the hydrodynamic radius and the green dashed line represents the DLS Count Rate. In (**b**), however, the green dashed line is the cumulative number fraction and the red line is the differential number fraction. In (**c**), the black line represents the feed solution chromatogram, the blue line is the permeate and the green and red line represent the retentate, with the green line being the retentate treated with Triton.

In addition to the chromatographic analysis methods, images of the LNP were also obtained using transmission electron microscopy (see Figure 7). These also show that the batchwise production produces both relatively large particles (Figure 7b) and smaller particles (Figure 7a), mirroring the broad particle size distribution.

The lipid nanoparticles generated on a batch scale produce relatively large particles, which are in the particle size range of 86–104 nm (the particle size corresponds to the particle diameter). Thus, a majority of the generated particles would not meet the QA requirements of having a maximum particle size of 100 nm. In contrast, around 90% of pDNA can be encapsulated and a PDI of maximum 0.027 can be achieved, which meets the QA requirements. The batch production of LNPs by pipetting is not expected to generate the required high mixing rates for small particles. In addition, the uptake and release of the mixture with the pipette leads to fluctuations in mixing and mixing speed, which results in the heterogeneous particle size distribution. The results of the batchwise LNP formulation

are in line with the expectations that relatively large particles with a large particle size distribution can be obtained during production with the pipette [21,22,25].

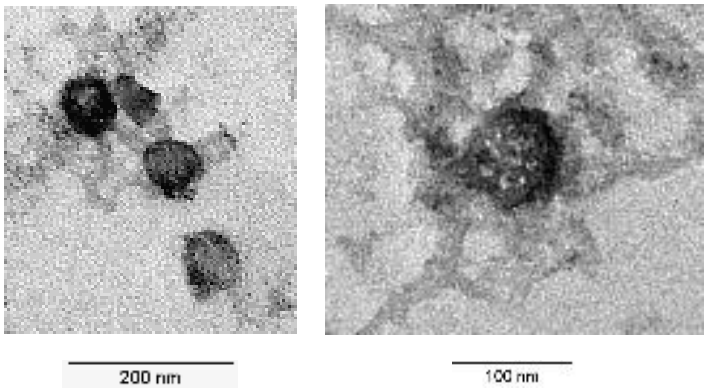

(**a**) (**b**)

Figure 7. TEM images of the produced LNPs. (**a**) Smaller particles; (**b**) large particle in the sample.

3.2. Continuous LNP Formation

A T-mixer was used for the continuous preparation of lipid nanoparticles containing pDNA, in which much higher mixing rates can be achieved than with the pipette [22,24,25]. The LNP are then diafiltered to remove the ethanol and bring the particles to physiological conditions. The chromatograms and particle size distributions of the continuous LNP formation are shown in Figure 8. Due to the higher mixing rate, particles with a hydrodynamic radius of 35 ± 2 nm, averaged over the whole process, are produced in contrast to the batchwise production. The particle radius remains almost constant during diafiltration after the T-mixer, and since it is smaller than the critical particle size, which corresponds to the particle diameter of 100 nm, it meets the quality requirements. Moreover, it is within the size range of the SARS-CoV-2 vaccine candidates nCoVsaRNA (Imperial College London) and ARCoV (Walvax Biotechnology), which have an average particle size of 75 nm and 89 nm, respectively [55,56]. For the Pfizer/BioNTech's Comirnaty mRNA vaccine, on which the composition of the LNP generated in this study is based, mean particle sizes ranging from 66 nm to 93.4 nm have been documented in the literature across different batches. Consequently, the mean particle size of the continuously produced LNP falls within this in range [57–59]. Furthermore, the constant high mixing rate can reduce the width of the particle size distribution to about 15 nm, as opposed to about 30 nm in the batchwise production. This also corresponds to the PDI, which is 0.004 ± 0.0003, in contrast to the minimum PDI of about 0.012 for batchwise production.

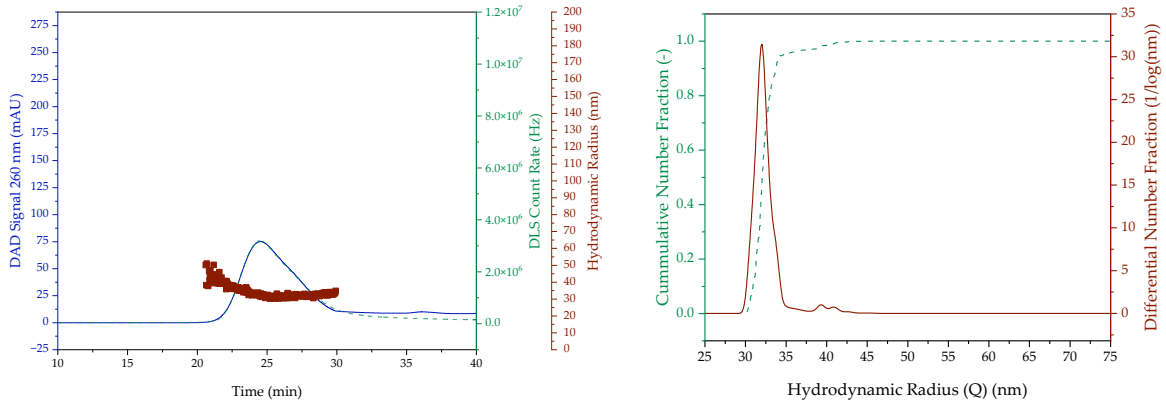

(**a**) (**b**)

Figure 8. *Cont.*

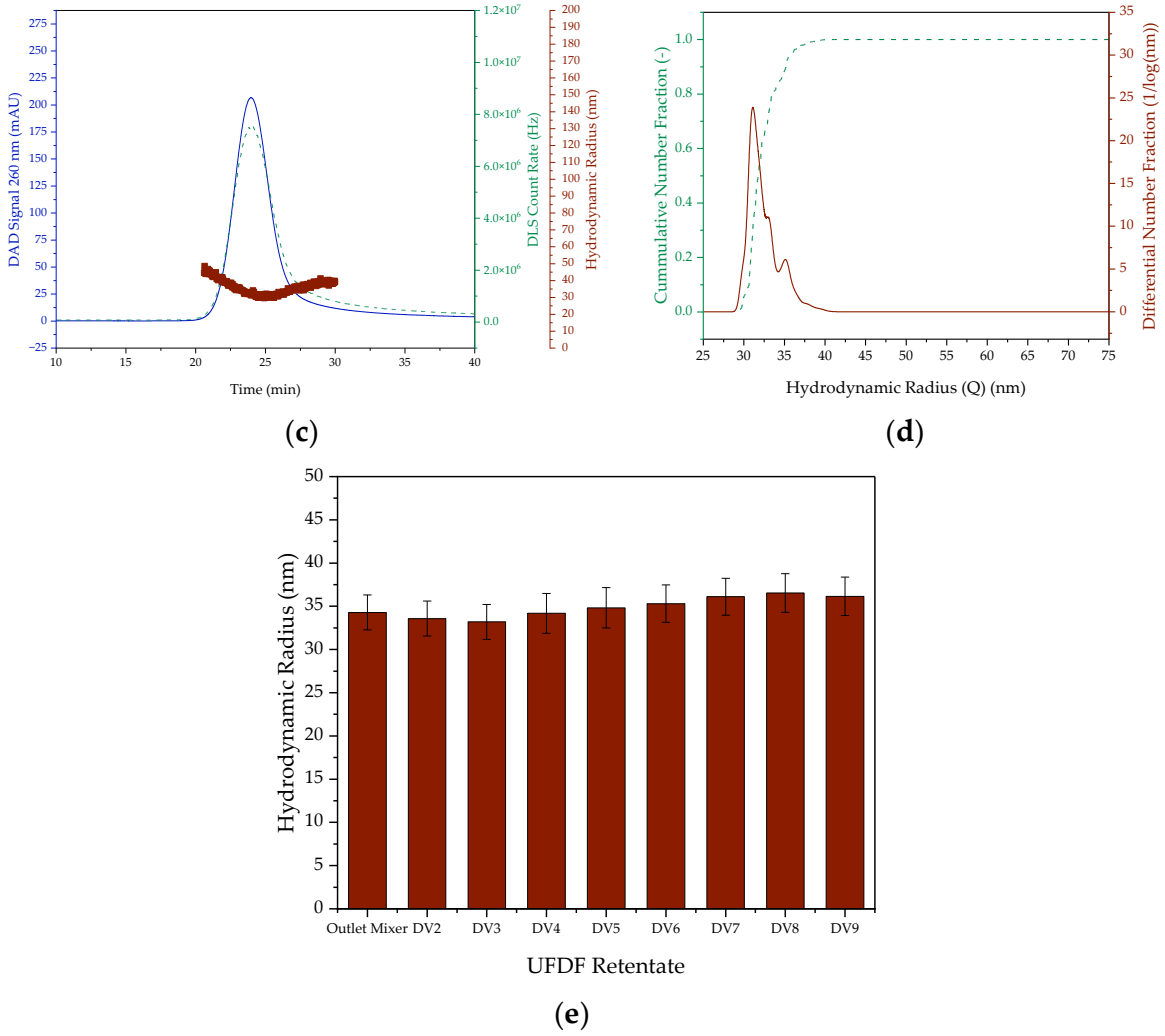

Figure 8. SEC chromatogram and DLS signal ((**a**) outlet of the T-Mixer (**b**) diafiltration volume 9) as well as the cumulative and differential distribution of hydrodynamic radius ((**c**) outlet of the T-Mixer (**d**) diafiltration volume 9) of LNP prepared continuously. (**e**) Hydrodynamic radius in the retentate versus the diafiltration volumes. The DAD Signal is colored blue. In (**a**,**c**), the red colored dots represent the hydrodynamic radius and the green dashed lines represent the DLS Count Rate. In (**b**,**d**), however, the green dashed line is the cumulative number fraction and the red line is the differential number fraction.

In contrast, the encapsulation efficiency of 88% after T-mixer (cf. Figure 9) is not significantly different from that generated in batch. It is also comparable to the EE of 88% of the mRNA vaccine Comirnaty generated by Pfizer/BioNTech [57] and the EE of approx. 90% of the SARS-CoV-2 vaccine candidate ARCoV (Walvax Biotechnology) [60]. Conveying the retentate in a circle during batch UF/DF presumably destroys some particles, so that the encapsulation efficiency decreases to a final 70% during the course of UF/DF (cf. Figure 9). With the intended use of continuous UF/DF via SPTFF, this is no longer expected, so that the high encapsulation efficiency can be preserved.

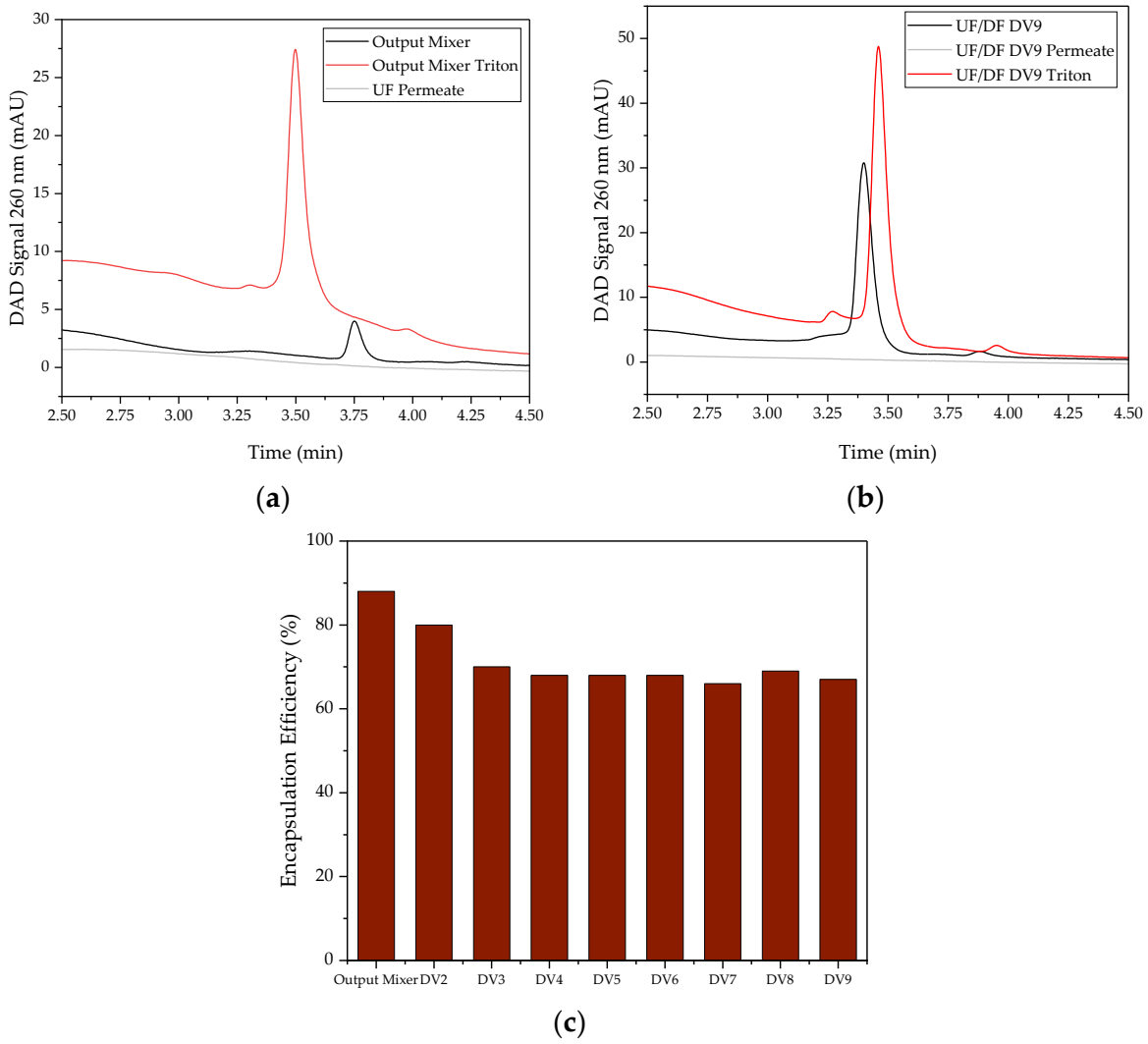

Figure 9. AEX chromatogram of UF/DF (**a**) outlet of the T-Mixer and (**b**) diafiltration volume 9. (**c**) Encapsulation efficiency over the diafiltration volumes. The grey lines represent the permeate, the black and red lines represent the retentate, with the red line being the retentate treated with Triton.

After T-mixing, the resulting LNP mixture was first mixed with 2 DV of exchange buffer to stop LNP formation reaction. Consequently, ultrafiltration (UF) was first performed to concentrate the solution back to a *VCF* of 1. Then, continuous buffer exchange was performed by diafiltration (DF). The course of the UF/DF is shown in Figure 10a. During UF/DF, a constant permeate flux (LMH) of 26 L/m^2/h on average was obtained. The TMP, however, increases from approx. 0.8 bar to approx. 1.3 bar during the UF/DF. In addition to removing the ethanol and buffering it into a physiological environment, UF/DF serves to separate unreacted lipids and thus increase the purity of the LNP. From the flowthrough peak of the AEX chromatogram containing the unreacted lipids in Figure 10, it can be seen that it decreases significantly in the retentate (b), whereas it increases in the permeate (c). Consequently, UF/DF can be used to increase the purity of the LNP.

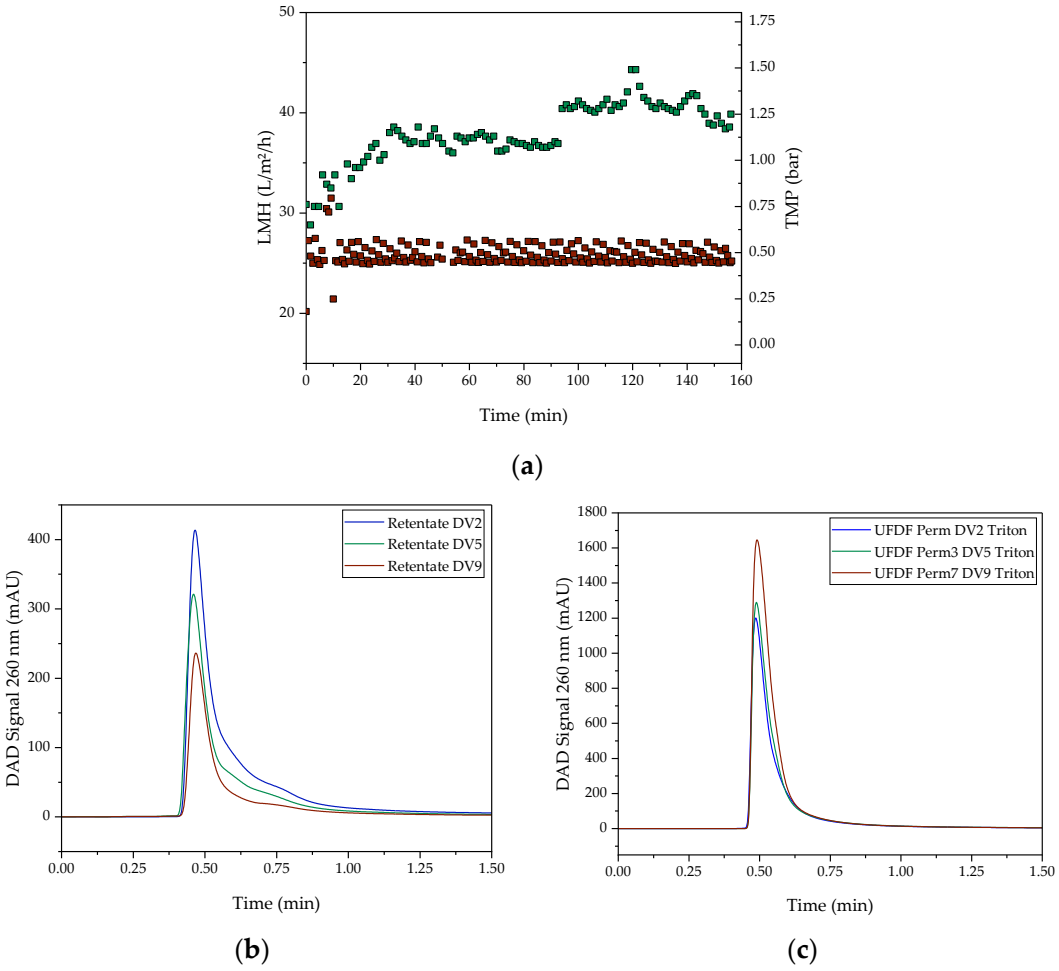

Figure 10. (**a**) Course of UF/DF (LMH (red points) and TMP (green points)). AEX chromatogram of UF/DF (**b**) retentate and (**c**) permeate.

In addition to the chromatographic analysis methods, images of the continuous produced LNP were also obtained using transmission electron microscopy (see Figure 11). Figure 11a shows the retentate after UF and Figure 11b the retentate at the end of DF. The TEM images also show that continuous production produces smaller particles than the batchwise production, as well as that the particle size does not change during UF/DF.

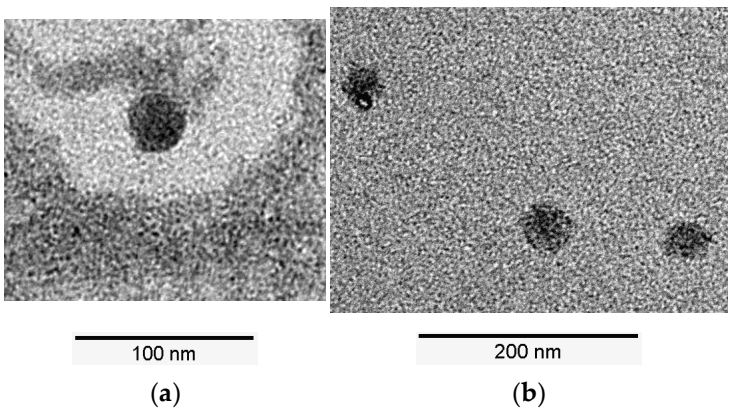

Figure 11. TEM images of the produced LNPs. (**a**) Retentate after ultrafiltration; (**b**) Retentate at the end of diafiltration.

3.3. LNP Quality in Batch and Continuous Mode

In this study, LNPs were first generated in 0.5 mL and 1.5 mL batch scales with and without (linearized) pDNA to be encapsulated. This was followed by a scale-up to a 12 mL scale, where pDNA was continuously encapsulated using a T-mixer. Table 3 shows the mean hydrodynamic radii, their minimum and maximum values, the resulting polydispersity indices and the obtained encapsulation efficiencies of the batchwise and continuous production of LNP.

Table 3. Comparison of mean hydrodynamic radius, minimum and maximum hydrodynamic radius, polydispersity index as well as obtained encapsulation efficiency of batchwise and continuously produced LNP in 0.5 mL, 1.5 mL and 12 mL scale with and without (linearized) pDNA.

Scale (mL)	Preparation Method	Nucleic Acid	Mean Hdrodynamic Radius (nm)	Min. Hydrodymanic Radius	Max. Hydrodynamic Radius	Polydispersity Index	Encapsulation Efficiency (%)
0.5	Batch	–	52 ± 6	44	69	0.012	–
0.5	Batch	pDNA	52 ± 6	45	66	0.012	–
1.5	Batch	–	48 ± 6	39	69	0.017	–
1.5	Batch	pDNA	43 ± 4	34	63	0.021	90
1.5	Batch	lin. pDNA	60 ± 10	36	75	0.027	32
12	Continuous	pDNA	35 ± 2	30	45	0.004	88

In the batchwise experiments, the smallest mean hydrodynamic radius generated is 43 nm in the 1.5 mL scale formulation of pDNA. This is almost 10 nm higher than that obtained in the continuous formulation. Both the widest particle size distribution and the largest mean particle size are in the LNP loaded with linearized pDNA, with all other batch experiments having a mean particle size of approximately 50 nm. Moreover, only 32% of the linear pDNA used could be encapsulated. In contrast, close to 90% of pDNA was encapsulated in both the batch and continuous formulations.

4. Discussion and Conclusions

In this study, lipid nanoparticles were first generated in a batchwise manner by pipetting. These would not meet the quality requirements with a particle size of around 86–104 nm and a particle size distribution width of around 30 nm. The heterogeneity and large particle size occur due to the too low mixing speed and fluctuating velocities during pipetting. This highlights the need for continuous LNP formation by microfluidic mixing to secure high-quality in-specification production [6].

Besides the non-continuous feasibility of pipetting and not meeting quality requirements, scale-up is required for continuous production of up to 10 million doses of mRNA within three days. For this purpose, a T-mixer was chosen and pDNA was encapsulated in a larger volume of 12 mL. Using the T-mixer, which induces rapid mixing by converting the laminar input streams into a turbulent stream at the mixing point [24,25], and controlling the volumetric flow rate more precisely, a much better and more homogeneous mixing of the aqueous and ethanol streams is achieved. This produces a much smaller particle size of 71 nm and a more homogeneous particle size distribution. Thus, the generated particles meet the quality requirements from Table 2. Moreover, the particle size and the achieved encapsulation efficiency of 88% coincide with the mean particle size range from 66 nm to 93 nm and the EE of 88% of Pfizer's mRNA vaccine, on which the composition of the LNPs in this study is based [57–59]. This suggests that the results of this study encapsulating the pDNA encoding the mRNA vaccine BNT162b2 are transferable to the encapsulation of mRNA.

With the continuous encapsulation of nucleic acids in lipid nanoparticles and the continuous production of mRNA in in vitro transcription, as demonstrated by Hengelbrock et al. [51], the basis for the holistic continuous production of mRNA is now in place. For a fully autonomous process, the incorporation of the process model of Helgers et al. [61] and a control strategy is essential. The latter was developed for the fully continuous mRNA process based on PID controllers by Schmidt et al. [62]. For model-based predictive

control, the implementation of PAT strategies is necessary [63], which has already been shown for diverse material systems [64–68]. The application of PAT also enables real-time-release-testing, which guarantees sufficient product quality and robustness [69–71]. This autonomous control, based on the integration of process model and PAT, could already be implemented in reality by Uhl et al. [72] for the production of pDNA and can now be transferred to the mRNA process based on this study and the studies by Hengelbrock et al. [51], Vetter et al. [73] and Schmidt et al. [62]. With such an autonomous continuous process, on the one hand, considerable time can be saved compared to the conventional process based on offline analytics [64,67]. On the other hand, a continuous process can reduce costs by increasing the time-space yield [61] and save labor and material costs through automation [62,74,75].

In summary, LNPs were continuously generated in a T-mixer in this study. These meet the quality requirements of an mRNA vaccine with an average particle size of 71 nm and an encapsulation efficiency of 88%. In addition, impurities such as unencapsulated lipids can be separated by the following UF/DF, which increases the purity of the generated LNP. In combination with continuous in vitro transcription as reported for the scalable mRNA machine [51] as well as SPTFF, this provides the basis for fully continuous bottleneck-free production of mRNA and other cell and gene therapy drug/vaccine candidates in a GMP- and QbD-compliant Biopharma 4.0 facility, enabled by predictive, validated process models and state-of-the-art PAT.

Author Contributions: Conceptualization, J.S.; software, process, analytics and experiments, A.H. and A.S.; writing—original draft preparation, A.H., A.S. and J.S.; writing—review and editing, A.H., A.S. and J.S.; supervision, J.S.; project administration, J.S. All authors have read and agreed to the published version of the manuscript.

Funding: This research received no external funding.

Institutional Review Board Statement: Not applicable.

Informed Consent Statement: Not applicable.

Data Availability Statement: Not applicable.

Acknowledgments: The authors would like to thank the team of the whole institute team including Heribert Helgers for *E.coli* cell line development, Alexander Uhl for aqueous two-phase extraction, Steffen Zobel-Roos for continuous chromatography and Alex Juckers for lyophilization; Mourad Mouellef and Thomas Knebel for their endless automation efforts; the mechanical and electrical workshop with Nils Hoffmann and Volker Strohmeyer for their fast-track assembly of LNP unit under the budgeting supervision of Claudia Lacheta; laboratory-head Frank Steinhäuser for his full-time trouble-shooting and total support. Martin Tegtmeier is also thanked as a qualified person for his regulatory guidance and supervision, as well as Peggy Knospe from the working group of Alfred Weber for the transmission electron microscope images. The authors acknowledge financial support from the Open Access Publishing Fund of the Clausthal University of Technology.

Conflicts of Interest: The authors declare no conflict of interest.

References

1. Burgos, R.M.; Badowski, M.E.; Drwiega, E.; Ghassemi, S.; Griffith, N.; Herald, F.; Johnson, M.; Smith, R.O.; Michienzi, S.M. The race to a COVID-19 vaccine: Opportunities and challenges in development and distribution. *Drugs Context* **2021**, *10*. [CrossRef] [PubMed]
2. Wang, J.; Peng, Y.; Xu, H.; Cui, Z.; Williams, R.O. The COVID-19 Vaccine Race: Challenges and Opportunities in Vaccine Formulation. *AAPS PharmSciTech* **2020**, *21*, 225. [CrossRef]
3. Rosa, S.S.; Nunes, D.; Antunes, L.; Prazeres, D.M.F.; Marques, M.P.C.; Azevedo, A.M. Maximizing mRNA vaccine production with Bayesian optimization. *Biotechnol. Bioeng.* **2022**, *119*, 3127–3139. [CrossRef]
4. Uttarilli, A.; Amalakanti, S.; Kommoju, P.-R.; Sharma, S.; Goyal, P.; Manjunath, G.K.; Upadhayay, V.; Parveen, A.; Tandon, R.; Prasad, K.S.; et al. Super-rapid race for saving lives by developing COVID-19 vaccines. *J. Integr. Bioinform.* **2021**, *18*, 27–43. [CrossRef] [PubMed]
5. Zhang, Y.; Hu, Y.; Tian, H.; Chen, X. Opportunities and Challenges for mRNA Delivery Nanoplatforms. *J. Phys. Chem. Lett.* **2022**, *13*, 1314–1322. [CrossRef] [PubMed]

6. Catignol, P.; Lim, H. Overcoming-Bottlenecks-in-mRNA-Manufacturing. Whitepaper. Available online: https://samsungbiologics.com/media/science-technology/overcoming-bottlenecks-in-mrna-manufacturing (accessed on 24 April 2023).
7. Carugo, D.; Bottaro, E.; Owen, J.; Stride, E.; Nastruzzi, C. Liposome production by microfluidics: Potential and limiting factors. *Sci. Rep.* **2016**, *6*, 25876. [CrossRef]
8. Maeki, M.; Kimura, N.; Sato, Y.; Harashima, H.; Tokeshi, M. Advances in microfluidics for lipid nanoparticles and extracellular vesicles and applications in drug delivery systems. *Adv. Drug Deliv. Rev.* **2018**, *128*, 84–100. [CrossRef] [PubMed]
9. Maherani, B.; Arab-Tehrany, E.; Mozafari, M.R.; Gaiani, C.; Linder, M. Liposomes: A Review of Manufacturing Techniques and Targeting Strategies. *Curr. Nanosci.* **2011**, *7*, 436–452. [CrossRef]
10. Blanco, E.; Shen, H.; Ferrari, M. Principles of nanoparticle design for overcoming biological barriers to drug delivery. *Nat. Biotechnol.* **2015**, *33*, 941–951. [CrossRef]
11. Widmer, J.; Thauvin, C.; Mottas, I.; van Nguyen, N.; Delie, F.; Allémann, E.; Bourquin, C. Polymer-based nanoparticles loaded with a TLR7 ligand to target the lymph node for immunostimulation. *Int. J. Pharm.* **2018**, *535*, 444–451. [CrossRef]
12. Schoenmaker, L.; Witzigmann, D.; Kulkarni, J.A.; Verbeke, R.; Kersten, G.; Jiskoot, W.; Crommelin, D.J.A. mRNA-lipid nanoparticle COVID-19 vaccines: Structure and stability. *Int. J. Pharm.* **2021**, *601*, 120586. [CrossRef] [PubMed]
13. Liang, F.; Lindgren, G.; Lin, A.; Thompson, E.A.; Ols, S.; Röhss, J.; John, S.; Hassett, K.; Yuzhakov, O.; Bahl, K.; et al. Efficient Targeting and Activation of Antigen-Presenting Cells In Vivo after Modified mRNA Vaccine Administration in Rhesus Macaques. *Mol. Ther.* **2017**, *25*, 2635–2647. [CrossRef]
14. Lindsay, K.E.; Bhosle, S.M.; Zurla, C.; Beyersdorf, J.; Rogers, K.A.; Vanover, D.; Xiao, P.; Araínga, M.; Shirreff, L.M.; Pitard, B.; et al. Visualization of early events in mRNA vaccine delivery in non-human primates via PET-CT and near-infrared imaging. *Nat. Biomed. Eng.* **2019**, *3*, 371–380. [CrossRef]
15. Hassett, K.J.; Benenato, K.E.; Jacquinet, E.; Lee, A.; Woods, A.; Yuzhakov, O.; Himansu, S.; Deterling, J.; Geilich, B.M.; Ketova, T.; et al. Optimization of Lipid Nanoparticles for Intramuscular Administration of mRNA Vaccines. *Mol. Ther. Nucleic Acids* **2019**, *15*, 1–11. [CrossRef] [PubMed]
16. Evers, M.J.W.; Kulkarni, J.A.; van der Meel, R.; Cullis, P.R.; Vader, P.; Schiffelers, R.M. State-of-the-Art Design and Rapid-Mixing Production Techniques of Lipid Nanoparticles for Nucleic Acid Delivery. *Small Methods* **2018**, *2*, 1700375. [CrossRef]
17. Reichmuth, A.M.; Oberli, M.A.; Jaklenec, A.; Langer, R.; Blankschtein, D. mRNA vaccine delivery using lipid nanoparticles. *Ther. Deliv.* **2016**, *7*, 319–334. [CrossRef] [PubMed]
18. Buschmann, M.D.; Carrasco, M.J.; Alishetty, S.; Paige, M.; Alameh, M.G.; Weissman, D. Nanomaterial Delivery Systems for mRNA Vaccines. *Vaccines* **2021**, *9*, 65. [CrossRef] [PubMed]
19. Yanez Arteta, M.; Kjellman, T.; Bartesaghi, S.; Wallin, S.; Wu, X.; Kvist, A.J.; Dabkowska, A.; Székely, N.; Radulescu, A.; Bergenholtz, J.; et al. Successful reprogramming of cellular protein production through mRNA delivered by functionalized lipid nanoparticles. *Proc. Natl. Acad. Sci. USA* **2018**, *115*, E3351–E3360. [CrossRef]
20. Ball, R.L.; Bajaj, P.; Whitehead, K.A. Achieving long-term stability of lipid nanoparticles: Examining the effect of pH, temperature, and lyophilization. *Int. J. Nanomed.* **2017**, *12*, 305–315. [CrossRef]
21. Cayman Chemical. A Guide to Lipid Nanoparticle Formulation: Basic Concepts & Preparation Procedures. Available online: https://www.biomol.com/dateien/Cayman{-}{-}A-Guide-to-Lipid-Nanoparticle-Formulation.pdf (accessed on 26 April 2023).
22. Cayabyab, C.; Brown, A.; Tharmarajah, A.T. mRNA Lipid Nanoparticles: Robust Low-Volume Production for Screening High-Value Nanoparticle Materials. Mrnaspark-Application Note-1018. Available online: https://www.precisionnanosystems.com/docs/default-source/pni-files/app-notes/spark-mrna-appnote-1018.pdf?sfvrsn=50662346_0 (accessed on 26 April 2023).
23. Kulkarni, J.A.; Darjuan, M.M.; Mercer, J.E.; Chen, S.; van der Meel, R.; Thewalt, J.L.; Tam, Y.Y.C.; Cullis, P.R. On the Formation and Morphology of Lipid Nanoparticles Containing Ionizable Cationic Lipids and siRNA. *ACS Nano* **2018**, *12*, 4787–4795. [CrossRef]
24. Kulkarni, J.A.; Tam, Y.Y.C.; Chen, S.; Tam, Y.K.; Zaifman, J.; Cullis, P.R.; Biswas, S. Rapid synthesis of lipid nanoparticles containing hydrophobic inorganic nanoparticles. *Nanoscale* **2017**, *9*, 13600–13609. [CrossRef]
25. Hirota, S.; de Ilarduya, C.T.; Barron, L.G.; Szoka, F.C. Simple mixing device to reproducibly prepare cationic lipid-DNA complexes (lipoplexes). *Biotechniques* **1999**, *27*, 286–290. [CrossRef] [PubMed]
26. Quagliarini, E.; Renzi, S.; Digiacomo, L.; Giulimondi, F.; Sartori, B.; Amenitsch, H.; Tassinari, V.; Masuelli, L.; Bei, R.; Cui, L.; et al. Microfluidic Formulation of DNA-Loaded Multicomponent Lipid Nanoparticles for Gene Delivery. *Pharmaceutics* **2021**, *13*, 1292. [CrossRef] [PubMed]
27. Kulkarni, J.A.; Witzigmann, D.; Leung, J.; van der Meel, R.; Zaifman, J.; Darjuan, M.M.; Grisch-Chan, H.M.; Thöny, B.; Tam, Y.Y.C.; Cullis, P.R. Fusion-dependent formation of lipid nanoparticles containing macromolecular payloads. *Nanoscale* **2019**, *11*, 9023–9031. [CrossRef]
28. Pilkington, E.H.; Suys, E.J.A.; Trevaskis, N.L.; Wheatley, A.K.; Zukancic, D.; Algarni, A.; Al-Wassiti, H.; Davis, T.P.; Pouton, C.W.; Kent, S.J.; et al. From influenza to COVID-19: Lipid nanoparticle mRNA vaccines at the frontiers of infectious diseases. *Acta Biomater.* **2021**, *131*, 16–40. [CrossRef] [PubMed]
29. Kulkarni, J.A.; Myhre, J.L.; Chen, S.; Tam, Y.Y.C.; Danescu, A.; Richman, J.M.; Cullis, P.R. Design of lipid nanoparticles for in vitro and in vivo delivery of plasmid DNA. *Nanomedicine* **2017**, *13*, 1377–1387. [CrossRef] [PubMed]
30. He, Z.; Hu, Y.; Nie, T.; Tang, H.; Zhu, J.; Chen, K.; Liu, L.; Leong, K.W.; Chen, Y.; Mao, H.-Q. Size-controlled lipid nanoparticle production using turbulent mixing to enhance oral DNA delivery. *Acta Biomater.* **2018**, *81*, 195–207. [CrossRef]

31. Mucker, E.M.; Karmali, P.P.; Vega, J.; Kwilas, S.A.; Wu, H.; Joselyn, M.; Ballantyne, J.; Sampey, D.; Mukthavaram, R.; Sullivan, E.; et al. Lipid Nanoparticle Formulation Increases Efficiency of DNA-Vectored Vaccines/Immunoprophylaxis in Animals Including Transchromosomic Bovines. *Sci. Rep.* **2020**, *10*, 8764. [CrossRef]
32. Sinegra, A.J.; Evangelopoulos, M.; Park, J.; Huang, Z.; Mirkin, C.A. Lipid Nanoparticle Spherical Nucleic Acids for Intracellular DNA and RNA Delivery. *Nano Lett.* **2021**, *21*, 6584–6591. [CrossRef]
33. Cui, L.; Renzi, S.; Quagliarini, E.; Digiacomo, L.; Amenitsch, H.; Masuelli, L.; Bei, R.; Ferri, G.; Cardarelli, F.; Wang, J.; et al. Efficient Delivery of DNA Using Lipid Nanoparticles. *Pharmaceutics* **2022**, *14*, 1698. [CrossRef]
34. Quagliarini, E.; Wang, J.; Renzi, S.; Cui, L.; Digiacomo, L.; Ferri, G.; Pesce, L.; de Lorenzi, V.; Matteoli, G.; Amenitsch, H.; et al. Mechanistic Insights into the Superior DNA Delivery Efficiency of Multicomponent Lipid Nanoparticles: An In Vitro and In Vivo Study. *ACS Appl. Mater. Interfaces* **2022**, *14*, 56666–56677. [CrossRef] [PubMed]
35. Food and Drug Administration. Pfizer-BioNTech COVID-19 Vaccine EUA Letter of Authorization reissued 05-10-2021. Available online: https://www.fda.gov/media/144412/download (accessed on 4 February 2023).
36. Mendonça, M.C.P.; Kont, A.; Kowalski, P.S.; O'Driscoll, C.M. Design of lipid-based nanoparticles for delivery of therapeutic nucleic acids. *Drug Discov. Today* **2023**, *28*, 103505. [CrossRef] [PubMed]
37. Cunha, S.; Costa, C.P.; Moreira, J.N.; Sousa Lobo, J.M.; Silva, A.C. Using the quality by design (QbD) approach to optimize formulations of lipid nanoparticles and nanoemulsions: A review. *Nanomedicine* **2020**, *28*, 102206. [CrossRef] [PubMed]
38. Caputo, F.; Arnould, A.; Bacia, M.; Ling, W.L.; Rustique, E.; Texier, I.; Mello, A.P.; Couffin, A.-C. Measuring Particle Size Distribution by Asymmetric Flow Field Flow Fractionation: A Powerful Method for the Preclinical Characterization of Lipid-Based Nanoparticles. *Mol. Pharm.* **2019**, *16*, 756–767. [CrossRef] [PubMed]
39. Daniel, S.; Kis, Z.; Kontoravdi, C.; Shah, N. Quality by Design for enabling RNA platform production processes. *Trends Biotechnol.* **2022**, *40*, 1213–1228. [CrossRef] [PubMed]
40. Fan, Y.; Marioli, M.; Zhang, K. Analytical characterization of liposomes and other lipid nanoparticles for drug delivery. *J. Pharm. Biomed. Anal.* **2021**, *192*, 113642. [CrossRef]
41. Hupfeld, S.; Holsaeter, A.M.; Skar, M.; Frantzen, C.B.; Brandl, M. Liposome size analysis by dynamic/static light scattering upon size exclusion-/field flow-fractionation. *J. Nanosci. Nanotechnol.* **2006**, *6*, 3025–3031. [CrossRef]
42. Jia, X.; Liu, Y.; Wagner, A.M.; Chen, M.; Zhao, Y.; Smith, K.J.; Some, D.; Abend, A.M.; Pennington, J. Enabling online determination of the size-dependent RNA content of lipid nanoparticle-based RNA formulations. *J. Chromatogr. B Analyt. Technol. Biomed. Life Sci.* **2021**, *1186*, 123015. [CrossRef]
43. Mildner, R.; Hak, S.; Parot, J.; Hyldbakk, A.; Borgos, S.E.; Some, D.; Johann, C.; Caputo, F. Improved multidetector asymmetrical-flow field-flow fractionation method for particle sizing and concentration measurements of lipid-based nanocarriers for RNA delivery. *Eur. J. Pharm. Biopharm.* **2021**, *163*, 252–265. [CrossRef]
44. Parot, J.; Caputo, F.; Mehn, D.; Hackley, V.A.; Calzolai, L. Physical characterization of liposomal drug formulations using multi-detector asymmetrical-flow field flow fractionation. *J. Control. Release* **2020**, *320*, 495–510. [CrossRef]
45. Zhang, J.; Haas, R.M.; Leone, A.M. Polydispersity characterization of lipid nanoparticles for siRNA delivery using multiple detection size-exclusion chromatography. *Anal. Chem.* **2012**, *84*, 6088–6096. [CrossRef]
46. Whitley, J.; Zwolinski, C.; Denis, C.; Maughan, M.; Hayles, L.; Clarke, D.; Snare, M.; Liao, H.; Chiou, S.; Marmura, T.; et al. Development of mRNA manufacturing for vaccines and therapeutics: mRNA platform requirements and development of a scalable production process to support early phase clinical trials. *Transl. Res.* **2022**, *242*, 38–55. [CrossRef] [PubMed]
47. Crawford, R.; Dogdas, B.; Keough, E.; Haas, R.M.; Wepukhulu, W.; Krotzer, S.; Burke, P.A.; Sepp-Lorenzino, L.; Bagchi, A.; Howell, B.J. Analysis of lipid nanoparticles by Cryo-EM for characterizing siRNA delivery vehicles. *Int. J. Pharm.* **2011**, *403*, 237–244. [CrossRef] [PubMed]
48. An, K.; Kurek, D.; Mahadeo, M.; Zhang, Y.; Thewalt, J.L.; Cullis, P.R.; Kulkarni, J.A. On the Influence of Nucleic Acid Backbone Modifications on Lipid Nanoparticle Morphology. *Langmuir* **2022**, *38*, 14036–14043. [CrossRef] [PubMed]
49. Gao, R.Y.; Riley, C.M.; Toth, E.; Blair, R.H.; Gerold, M.N.; McCormick, C.; Taylor, A.W.; Hu, T.; Rowlen, K.L.; Dawson, E.D. Rapid Identity and Quantity CQA Test for Multivalent mRNA Drug Product Formulations. *Vaccines* **2022**, *10*, 1704. [CrossRef] [PubMed]
50. Malburet, C.; Leclercq, L.; Cotte, J.-F.; Thiebaud, J.; Bazin, E.; Garinot, M.; Cottet, H. Size and Charge Characterization of Lipid Nanoparticles for mRNA Vaccines. *Anal. Chem.* **2022**, *94*, 4677–4685. [CrossRef] [PubMed]
51. Hengelbrock, A.; Schmidt, A.; Helgers, H.; Vetter, F.L.; Strube, J. Scalable mRNA Machine for Regulatory Approval of Variable Scale between 1000 Clinical Doses to 10 Million Manufacturing Scale Doses. *Processes* **2023**, *11*, 745. [CrossRef]
52. van der Bruggen, B. Microfiltration, ultrafiltration, nanofiltration, reverse osmosis, and forward osmosis. In *Fundamental Modelling of Membrane Systems*; Elsevier: Amsterdam, The Netherlands, 2018; pp. 25–70. ISBN 9780128134832.
53. Russo, T. *A Hands-On Guide to Ultrafiltration/Diafiltration Optimization Using Pellicon® Cassettes: Application Note*; EMD Millipore Corporation: Burlington. MA, USA, 2013.
54. Jung, H.N.; Lee, S.-Y.; Lee, S.; Youn, H.; Im, H.-J. Lipid nanoparticles for delivery of RNA therapeutics: Current status and the role of in vivo imaging. *Theranostics* **2022**, *12*, 7509–7531. [CrossRef]
55. McKay, P.F.; Hu, K.; Blakney, A.K.; Samnuan, K.; Brown, J.C.; Penn, R.; Zhou, J.; Bouton, C.R.; Rogers, P.; Polra, K.; et al. Self-amplifying RNA SARS-CoV-2 lipid nanoparticle vaccine candidate induces high neutralizing antibody titers in mice. *Nat. Commun.* **2020**, *11*, 3523. [CrossRef]

56. Zhang, H.; Rombouts, K.; Raes, L.; Xiong, R.; de Smedt, S.C.; Braeckmans, K.; Remaut, K. Fluorescence-Based Quantification of Messenger RNA and Plasmid DNA Decay Kinetics in Extracellular Biological Fluids and Cell Extracts. *Adv. Biosyst.* **2020**, *4*, e2000057. [CrossRef]
57. Kudsiova, L.; Lansley, A.; Scutt, G.; Allen, M.; Bowler, L.; Williams, S.; Lippett, S.; Stafford, S.; Tarzi, M.; Cross, M.; et al. Stability testing of the Pfizer-BioNTech BNT162b2 COVID-19 vaccine: A translational study in UK vaccination centres. *BMJ Open Sci.* **2021**, *5*, e100203. [CrossRef]
58. Szebeni, J.; Kiss, B.; Bozó, T.; Turjeman, K.; Levi-Kalisman, Y.; Barenholz, Y.; Kellermayer, M. New insights into the structure of Comirnaty COVID-19 vaccine: A theory on soft nanoparticles with mRNA-lipid supercoils stabilized by hydrogen bonds. *bioRxiv* **2022**.
59. Thaller, A.; Schmauder, L.; Frieß, W.; Winter, G.; Menzen, T.; Hawe, A.; Richter, K. SV-AUC as a stability-indicating method for the characterization of mRNA-LNPs. *Eur. J. Pharm. Biopharm.* **2023**, *182*, 152–156. [CrossRef] [PubMed]
60. Zhao, H.; Wang, T.-C.; Li, X.-F.; Zhang, N.-N.; Li, L.; Zhou, C.; Deng, Y.-Q.; Cao, T.-S.; Yang, G.; Li, R.-T.; et al. Long-term stability and protection efficacy of the RBD-targeting COVID-19 mRNA vaccine in nonhuman primates. *Signal Transduct. Target. Ther.* **2021**, *6*, 438. [CrossRef] [PubMed]
61. Helgers, H.; Hengelbrock, A.; Schmidt, A.; Strube, J. Digital Twins for Continuous mRNA Production. *Processes* **2021**, *9*, 1967. [CrossRef]
62. Schmidt, A.; Helgers, H.; Vetter, F.L.; Zobel-Roos, S.; Hengelbrock, A.; Strube, J. Process Automation and Control Strategy by Quality-by-Design in Total Continuous mRNA Manufacturing Platforms. *Processes* **2022**, *10*, 1783. [CrossRef]
63. Schmidt, A.; Helgers, H.; Lohmann, L.J.; Vetter, F.; Juckers, A.; Mouellef, M.; Zobel-Roos, S.; Strube, J. Process analytical technology as key-enabler for digital twins in continuous biomanufacturing. *J. Chem. Technol. Biotechnol.* **2022**, *97*, 2336–2346. [CrossRef]
64. Helgers, H.; Hengelbrock, A.; Schmidt, A.; Vetter, F.L.; Juckers, A.; Strube, J. Digital Twins for scFv Production in Escherichia coli. *Processes* **2022**, *10*, 809. [CrossRef]
65. Helgers, H.; Hengelbrock, A.; Schmidt, A.; Rosengarten, J.; Stitz, J.; Strube, J. Process Design and Optimization towards Digital Twins for HIV-Gag VLP Production in HEK293 Cells, including Purification. *Processes* **2022**, *10*, 419. [CrossRef]
66. Helgers, H.; Schmidt, A.; Strube, J. Towards Autonomous Process Control—Digital Twin for CHO Cell-Based Antibody Manufacturing Using a Dynamic Metabolic Model. *Processes* **2022**, *10*, 316. [CrossRef]
67. Hengelbrock, A.; Helgers, H.; Schmidt, A.; Vetter, F.L.; Juckers, A.; Rosengarten, J.F.; Stitz, J.; Strube, J. Digital Twin for HIV-Gag VLP Production in HEK293 Cells. *Processes* **2022**, *10*, 866. [CrossRef]
68. Mouellef, M.; Szabo, G.; Vetter, F.L.; Siemers, C.; Strube, J. Artificial Neural Network for Fast and Versatile Model Parameter Adjustment Utilizing PAT Signals of Chromatography Processes for Process Control under Production Conditions. *Processes* **2022**, *10*, 709. [CrossRef]
69. FDA perspective on continuous manufacturing. In Proceedings of the IFPAC Annual Meeting, Baltimore, MD, USA, 22–25 January 2012.
70. ICH Expert Working Group. *Pharmaceuticel Development Q8(R2): ICH Harmonised Tripartite Guideline*; ICH Expert Working Group: Geneva, Switzerland, 2009.
71. ICH Expert Working Group. *ICH Q12—Technical and Regulatory Considerations for Pharmaceutical Product Lifecycle Management*; ICH Expert Working Group: Geneva, Switzerland, 2020.
72. Uhl, A.; Schmidt, A.; Hlawitschka, M.W.; Strube, J. Autonomous Liquid–Liquid Extraction Operation in Biologics Manufacturing with Aid of a Digital Twin including Process Analytical Technology. *Processes* **2023**, *11*, 553. [CrossRef]
73. Vetter, F.L.; Zobel-Roos, S.; Mota, J.P.B.; Nilsson, B.; Schmidt, A.; Strube, J. Toward Autonomous Production of mRNA-Therapeutics in the Light of Advanced Process Control and Traditional Control Strategies for Chromatography. *Processes* **2022**, *10*, 1868. [CrossRef]
74. Schmidt, A.; Helgers, H.; Vetter, F.L.; Juckers, A.; Strube, J. Digital Twin of mRNA-Based SARS-COVID-19 Vaccine Manufacturing towards Autonomous Operation for Improvements in Speed, Scale, Robustness, Flexibility and Real-Time Release Testing. *Processes* **2021**, *9*, 748. [CrossRef]
75. Schmidt, A.; Helgers, H.; Vetter, F.L.; Juckers, A.; Strube, J. Fast and Flexible mRNA Vaccine Manufacturing as a Solution to Pandemic Situations by Adopting Chemical Engineering Good Practice—Continuous Autonomous Operation in Stainless Steel Equipment Concepts. *Processes* **2021**, *9*, 1874. [CrossRef]